JOURNAL OF TISSUE ENGINEERING AND REGENERATIVE MEDICINE
J Tissue Eng Regen Med 2015; **9**: 41–54.
Published online 29 October 2012 in Wiley Online Library (wileyonlinelibrary.com) **DOI:** 10.1002/term.1613

RESEARCH ARTICLE

Comparative effect of human and *Trypanosoma cruzi* calreticulin in wound healing

J. Ignacio Arias[1]*, Caroll Sepulveda[1], Patricia Bravo[1], Christopher Hamilton-West[1], Ismael Maldonado[2] and Arturo Ferreira[2]

[1]*Faculty of Veterinary and Animal Science, University of Chile, Santiago, Chile*
[2]*Immunology Disciplinary Programme, ICBM, Faculty of Medicine, Universidad de Chile, Santiago, Chile*

Abstract

In orthopaedics, the use of factors that enhance granulation tissue formation and prevent or delay new bone regeneration is sometimes desirable. Calreticulin (CRT), a unique endoplasmic reticulum luminal Ca^{2+}-binding chaperone widely distributed in eukaryotic cells, is involved in many cellular functions. Among them, CRT has an important influence in cutaneous wound healing and diverse processes associated with cutaneous repair, inhibition of angiogenesis, promotion of cell adhesion and antitumour effect. One of the molecules involved in several aspects of the host–parasite interplay is *Trypanosoma cruzi* calreticulin (TcCRT), which is highly homologous to human calreticulin (HuCRT). Here, recombinant (r)HuCRT and rTcCRT are compared on their abilities to affect fibroblast behaviour in a scratch plate assay, and wound healing in *in vivo* skin rat models. In molar terms, rTcCRT is three orders of magnitude more efficient than rHuCRT in increasing proliferation and migration of human fibroblasts *in vitro*. A similar effect was observed *in vivo* on rat skin wounds and inhibition of bone gap bridging in rabbit unicortical bone osteotomies. Copyright © 2012 John Wiley & Sons, Ltd.

Received 28 September 2011; Revised 21 June 2012; Accepted 25 August 2012

Keywords **Trypanosoma cruzi; calreticulin; fibroblast; proliferation; migration; cell culture**

1. Introduction

In orthopaedics the main efforts are focused on achieving the regeneration of bone or joint injuries. However, in veterinary orthopaedics the opposite may be required. This is the case in radius curvus, where ulnar ostectomy is performed to free the proximal end of the ulna from the radial shaft, allowing the normal growth of the radius with the formation of interposed granulation tissue. A similar situation occurs in osteoarthritis in hip dysplasias, where the femoral head and neck are excised to control pain. This is accomplished by means of inducing a fibrous pseudoarthrosis formation in the coxo-femoral joint, thus effectively functioning as a salvage hip joint (Lippincott, 1992). Therefore, the use of factors that enhance granulation tissue formation and avoid or delay new bone bridging is desirable (Arias *et al*., 2008). Such granulation tissue is normally found during natural skin wound healing (Nguyen *et al*., 2009) and can be modulated by the administration of different chemical agents (Bae *et al*., 2005; Okwueze *et al*., 2007).

Found originally in rabbit muscle cells (Ostwald and MacLennan, 1974), calreticulin (CRT) is a unique endoplasmic reticulum (ER) Ca^{2+}-binding chaperone widely distributed in eukaryotic cells. It plays a role in many cellular functions, such as lectin-like chaperoning, Ca^{2+} storage, and signalling and regulation of gene expression (Michalak *et al*., 2009). CRT is expressed in different mammalian cells and its extracellular functions, have been tested in several *in vivo* and *in vitro* assays, showing that CRT has an important influence in cutaneous wound healing and diverse processes associated with cutaneous repair (Gold *et al*., 2006, 2010; Nanney *et al*., 2008), inhibition of angiogenesis (López *et al*., 2010; Toledo *et al*., 2010), promotion of cell adhesion (Papp *et al*., 2007) and antitumour effects (López *et al*., 2010; Toledo *et al*., 2010; Ramírez *et al*., 2011a).

Extracellular biological activities of CRT are mainly related to cellular adhesion, migration and phagocytosis, which are critical aspects of wound healing (Nguyen

*Correspondence to: J. Ignacio Arias, Faculty of Veterinary Science, Universidad de Chile, Casilla 2 Correo 15, La Granja, Santiago, Chile. E-mail: joarias@uchile.cl

et al., 2009). In fact, CRT was originally shown to be the biologically active component of hyaluronic acid isolates from fetal sheep skin that accelerated wound healing in animal experimental models of cutaneous repair (Burd *et al.*, 1991; Bakshandeh *et al.*, 1992; Cabrera *et al.*, 1995).

Increasing interest on this molecule comes from its discovery in the flagellated protozoan *Trypanosoma cruzi* (Aguillón *et al.*, 2000; Ramos *et al.*, 1991), a parasite responsible for Chagas' disease (Chagas, 1909). Unlike other trypanosomes, such as blood-borne *Leishmania* and *Trypanosoma brucei*, *T. cruzi* cycles between extracellular and intracellular stages. This constant seeking of the microorganism to hide inside mammalian cells is linked to the fact that intracellular parasites are less susceptible to drugs and humoral immune responses (Ferreira *et al.*, 2004b). *T. cruzi* molecules involved in immune and non-immune modulation of the chronic progression of this disease are important, not only to understand the basic biological aspects of its relationships with the host but also to allow the development of possible treatment strategies (Ramírez *et al.*, 2011a).

One of the molecules involved in several functions of host–parasite interactions is *T. cruzi* calreticulin (TcCRT) (Ferreira *et al.*, 2004a, 2004b; Ribeiro *et al.*, 2009; López *et al.*, 2010; Valck *et al.*, 2010; Ramírez *et al.*, 2011a, 2011b). TcCRT is 50% homologous to human calreticulin (HuCRT), an exceedingly pleiotropic chaperone molecule (Ferreira *et al.*, 2004a). This protein has been found inside the ER, on the surface of the parasite membrane and outside the parasite (Ferreira *et al.*, 2004b; Ramírez *et al.*, 2011b). Extracellular TcCRT functions, such as antiangiogenic effects, have also been reported (Ferreira *et al.*, 2005; Molina *et al.*, 2005; Ramírez *et al.*, 2011a).

TcCRT shares several functions with HuCRT. However, some differences have been reported, e.g. TcCRT does not bind to laminin (López *et al.*, 2010) or to H-Ficolin. Functionally, TcCRT is more efficient, in equimolar terms, than its human counterpart. Thus TcCRT displays stronger antiangiogenic and anti-tumoural effects, as determined in *ex vivo* and *in vitro* experimental set-ups (López *et al.*, 2010). The sharing of several functional domains by vertebrate and parasite CRT, and the differences of efficiency in the concentrations needed to evidence their effects on different tissues, encourages further investigation to understand the function of this molecule in wound healing.

Chitosan, a mucopolysaccharide with structural characteristics similar to glycosamines, is a natural cationic polymer, biologically renewable, biodegradable, biocompatible, non-antigenic, non-toxic and biofunctional. This biopolymer, produced by deacetylation of chitin, is derived from the exoskeleton of crustaceans. Chitosan has been used as a wound dressing in burns, where it promotes proliferation and activation of inflammatory cells in granulation tissue, thus accelerating wound healing (Ueno *et al.*, 1999, 2001; Howling *et al.*, 2001; Lai *et al.*, 2003). Other laboratories (Sezer *et al.*, 2007, 2008a, 2008b) have also successfully used a chitosan-based matrix containing Fucoidan as an approach to treat skin wounds.

The role of mammalian CRT in wound healing is well established (Gold *et al.*, 2010). Here, rHuCRT and rTcCRT, absorbed in a chitosan sponge, are compared on their abilities to modulate skin and bone wound healing, both *in vitro* and *in vivo*.

2. Materials and methods

2.1. Calreticulin

rTcCRT was cloned, amplified and expressed as previously described (Ferreira *et al.*, 2004b). Briefly, DNA coding for TcCRT was isolated from a genomic library in the Xgt11 phage. TcCRT, without its leader and KEDL endoplasmic reticulum retention sequence, was amplified by PCR and ligated in the pET-28b^{+} vector (Novagen, Darmstadt, Germany) in *Eco*RI restriction sites. DNA coding for HuCRT (a kind gift of Professor Wilhelm Schwaeble, Leicester University, UK) was also amplified and expressed following standard procedures.

2.2. Fibroblasts

Human skin fibroblasts (kindly provided by Dr M. Fernandez, Institute of Nutrition and Food Technology, University of Chile) were obtained from fresh child preputial skin, as published elsewhere (Palma *et al.*, 2002). The dermal fibroblasts were grown in complete Eagle's minimal essential medium (MEM); containing 10% fetal bovine serum (FBS) 2 mM glutamine and antibiotic–antimycotic (ABAM). At 60–70% confluence, the cells were washed with phosphate-buffered saline (PBS) and removed for replating with 0.25% trypsin/2.21 mM EDTA (Mediatech); the trypsin was neutralized with 10% FBS in MEM and the cells centrifuged and resuspended in complete MEM at densities described below.

2.3. Wound-healing scratch plate assay

The wound-healing scratch plate assay is a well-accepted *in vitro* correlate of important parameters of the *in vivo* process (Nanney *et al.*, 2008). Primary cultures of dermal fibroblasts were seeded in 24-well tissue culture plates at 1.0×10^4/well in complete medium and the cells grown to approximately 70–80% confluence. Scratches in each well were performed by drawing a line down the centre of the well with a 200 µl plastic pipette and the plate washed with serum-free MEM to remove the displaced cells. Then increasing concentrations (0–40 µg/ml) of HuCRT and TcCRT solutions in PBS were added to fibroblasts in quadruplicate wells. After 24 h of incubation, the cells were stained with 0.025% Coomassie blue in 10% acetic acid/45% methanol for 10 min and washed twice with PBS. The wells were viewed with an inverted light microscope (Nikon TMS) and images captured using Motic Images Plus v 2.0. Scratch closure (cellular migration)

DOI: 10.1002/term

was determined using National Institutes of Health ImageJ v 1.37 software, by colouring the cells migrating into the wounds area (Figure 1) and calculating the percentage of closure according to the following equation:

$$\%\,\text{closure}\,\frac{\text{number of pixels of the coloured migrating cells}}{\text{number of pixels in the scratch area at time 0}}\times 100$$

2.4. Cell proliferation assay (MTT)

For cell proliferation estimation, a colorimetric MTT method (Invitrogen®) was used. Yellow MTT [3-(4,5-dimethylthiazol-2-yl)-2,5-diphenyltetrazolium bromide], a tetrazole, is reduced to purple formazan in the mitochondria of living cells. This reduction takes place only when mitochondrial reductase enzymes are active, and therefore conversion can be directly related to the number of viable (living) cells. Briefly, the primary cultures of dermal fibroblasts were seeded in 24-well tissue culture plates at 2.0×10^4/well and cultured for 24 h at 37 °C in 5% CO_2. Then, 1 ml culture medium plus 100 µl 0.5% MTT were added and incubated for an additional 3 h. After removing the MTT reagent, a lysis solution (10% SDS in DMSO/HCl) was added and incubated for 5 min to allow cell lysis. 200 µl lysate were added to 96 micro-ELISA plate wells and then absorbance was read at 550 nm on an ELISA plate reader to determine the cell number ± standard error of the mean (SE) per construct by comparison to a standardized cell proliferation curve.

2.5. Preparation of glutaraldehyde-crosslinked chitosan sponges

The scaffolds were prepared as follows: a solution of 2% low molecular weight chitosan (20–200 cps; Aldrich), 86% deacetylated, in 5% acetic acid was shaken for 24 h at room temperature and then filtered to remove non-dissolved chitosan and impurities (Fernández *et al*., 2012). Chitosan sponges were obtained by freeze-drying the chitosan solution with the addition of 0–5% glutaraldehyde (crosslinker agent) in liquid nitrogen and then lyophilized repeatedly for 48 h. 4 mm^2 pieces, with an average weight of 20 µg, were then cut and individually packed and sterilized by EThO gas. A single batch of this preparation was used in all experiments reported herein.

2.6. Swelling test of crosslinked chitosan sponges

The swelling ability of glutaraldehyde-crosslinked chitosan sponges was determined by incubating the sponges with 0–5% glutaraldehyde in simulated body fluid (SBF), pH 7.4, at 37 °C. A known weight of the sponge was placed in the medium. The wet weight of the sponge was determined at 12, 24, 48 and 96 h by first removing water on the surface with filter paper and then weighing immediately on an electronic balance. The percentage water absorption of chitosan sponges in the medium was calculated as follows:

$$E_{sw} = [W_e - W_0/W_0] \times 100$$

where E_{sw} is the percentage water absorption of a sponge at equilibrium, W_e denotes the weight of the sponge at equilibrium water absorption and W_0 is the initial weight of the sponge. Each experiment was repeated three times, and the average value was taken as the percentage water uptake.

2.7. Chitosan sponge SEM morphology

The morphology of chitosan sponge was investigated by scanning electron microscopy (SEM; Tesla BS 343A). The specimens were coated with a 20 nm thick gold layer, using an EMS-550 automated sputter-coater at 25 mA for 4 min. Surface morphology, pore size and structure of the scaffolds were examined under SEM, operating at 15 kV.

2.8. Chitosan sponges loaded with HuCRT and TcCRT

Loading of CRT in each chitosan sponge was accomplished by soaking the 20 µg chitosan sponge cubes with 40 µl low (2.5 ng/µl) and high (1 µg/µl) doses of rHuCRT and rTcCRT. After each sponge was soaked, it was implanted in the corresponding skin wound or bone defect, as

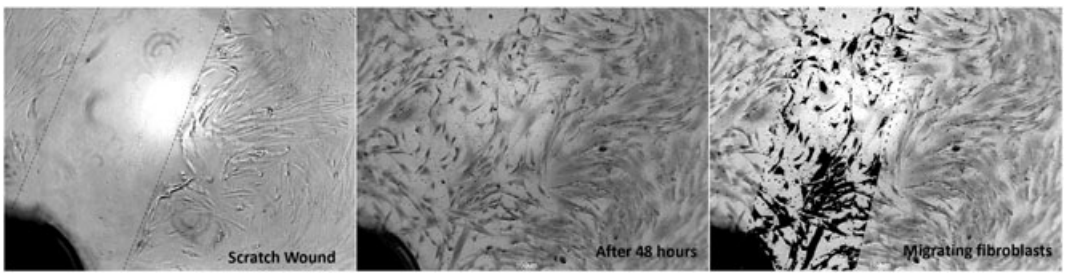

Figure 1. The wound-healing scratch plate assay, as applied to the CRT study: digital microphotographs (×40) of a human fibroblasts primary culture with scratch plate wound not stained (left), after 48 h of culture and stained with Coomassie blue (centre) and with dark digital stain of the migrating fibroblast in the scratch wound area (right)

DOI: 10.1002/term

described in the next section. After 24 h of incubation, the cells were stained with 0.025% Coomassie blue in 10% acetic acid/45% methanol for 10 min and washed twice with PBS. The wells were viewed with an inverted light microscope (Nikon TMS) and images captured using Motic Images Plus v 2.0. Scratch closure (cellular migration) was determined using National Institutes of Health ImageJ v 1.37 software, by colouring the cells migrating into the wounds area (Figure 1) and calculating the percentage of closure according to the equation shown in section 2.3.

2.9. *In vivo* skin wound assay in rat model

Adult male Sprague-Dawley rats weighing 300–350 g were divided into two experimental groups (three rats/group). The rats were anaesthetized by inhalation anaesthesia with 2% isoflurane. The dorsal skin was shaved, washed with 0.05% chlorhexidine and wiped with 75% ethanol solution. Using a 5 mm diameter circular excisional biopsial punch, six full-thickness skin wounds were made in the dorsal thorax, three on each side, and small subcutaneous blunt dissection was carried out lateral to the skin wounds to bed the chitosan sponge implants under the excision. Chitosan sponges were used alone or loaded with 40 μl high (1.0 μg/μl) and low (2.5 ng/μl) concentrations of HuCRT and TcCRT, as shown in Figure 2.

These wounds were allowed to heal by secondary intention for 5 and 10 days. At the end of each experiment, wounds with an adjacent margin of normal skin were excised, divided vertically into three full-thickness tissue sections/wound, fixed in 10% neutral buffered formalin for 24 h and then embedded in paraffin, and 5.0 μm tissue sections were cut and mounted on glass slides for histological analysis.

All protocols for both rat and rabbit studies, as described above, were approved by the Committee of Animal Bioethics of the Faculty of Medicine, University of Chile, which is in accordance with the International Guiding Principles for Biomedical Research Involving Animals, developed by the Council for International Organizations of Medical Sciences (CIOMS).

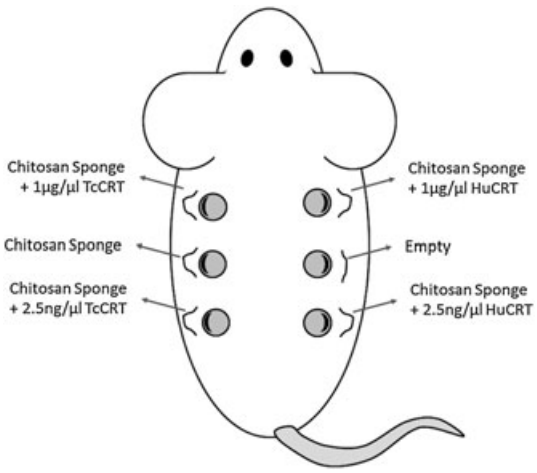

Figure 2. ***In vivo*** **rat experimental wound distribution. Six full-thickness 5 mm skin wounds were performed in the dorsal thorax (three on each side) in each rat. Chitosan sponges were used alone or loaded with 40 μl high (1.0 μg/μl) and low (2.5 ng/μl) concentrations of either rHuCRT or rTcCRT**

2.10. Granulation tissue formation/neodermal depth assessment

Granulation tissue thickness was measured in haematoxylin and eosin (H&E)-stained tissue slides. The granulation tissue converts into a neodermis as re-epithelialization is nearly complete, as measured by dermal depth. Neodermal depth measurements extend from the dermal–epidermal junction down to the intersection of the newly formed granulation tissue with the adjacent underlying discontinuous panniculus muscle. The results were expressed in μm and compared with normal hypodermis depth (1.5 ± 0.62 mm).

2.11. Dermis cell density comparison

Dermis maturity is reflected by dense connective tissue that contains collagen and elastin fibres, and fewer fibroblasts, macrophages and adipocytes, as well as nerves, glands and hair follicles. The cell number present between the collagen fibres of the dermis connective tissue of the wound site was determined by digitally colouring their nuclei, while density was expressed as number of cells/mm^2. Data were compared with the average number of cells of normal rat dermis (0.9 cells/ mm^2).

2.12. Re-epithelialization histological analysis

Tissue sections were stained with H&E and the extent of re-epithelialization and height of the stratified squamous epithelium of the skin wounds determined by morphometric analysis. Serial images of wounds were captured under a Nikon Eclipse E-400 light microscope and displayed on a video screen, using a NIKON DS-SMc camera. Quantitative measurements were performed using Nikon Image System Elements Basic Research v 3.2 digitalizing software.

The extent of re-epithelialization of the wounds was determined after 5 and 10 days of healing in the rats. This was achieved by measuring a composite of newly resurfaced epidermis that migrated over the wounds from the wound edges and epithelial islands derived from surviving epithelium that migrated upward from hair follicles. These measurements considered the total wound length. The data were expressed as a percentage of resurfacing, as described elsewhere (Okwueze *et al.*, 2007).

2.13. *In vivo* rabbit limbs bone defects

Six 2–3 month-old male New Zealand White rabbits, weight 3-4 kg, were divided into three time period groups (one defect for each tibia, femur and humerus). The rabbits were

DOI: 10.1002/term

anaesthetized and maintained with isoflurane inhalation, and operated under standard aseptic techniques. Limbs were shaved and washed with 0.5% chlorhexidine gluconate. The bone surfaces were exposed via a skin incision and subperiosteal dissection. Unicortical bone defects were made with a high-torque, low-speed trephine burr (5 mm outer diameter) under constant saline irrigation. On each rabbit, one bone defect (negative control) was left to heal spontaneously, while the other five were implanted with 4 mm^3 CRT-free chitosan sponges, or chitosan sponges embedded with 40 μl 1.0 μg/ml or 2.5 ng/ml of either rTcCRT or rHuCRT, respectively. Wound closure was accomplished by a simple discontinuous subcutaneous pattern (4-0 polyglactin 910) and with a simple discontinuous skin pattern (4-0 nylon). Ketoprofen (1 mg/kg every 24 h for 3 days) and tramadol (3 mg/kg every 24 h for 7 days) were administrated as anti-inflammatory and analgesic treatments, respectively. The rabbits were injected with 5 mg/kg enrofloxacin, daily for a week. The animals were euthanized at 1, 2 and 4 weeks. Implanted and negative control limb bones were retrieved with the surrounding soft tissues and fixed in a 10% formaldehyde for 2 h. Then they were trimmed to 2–3 cm sections (to approximately 0.5 cm above and below the defect site) using an Isomed Diamond Blade Low Speed Saw (Buehler), and then fixed in 10% formaldehyde for 1 week. After washing with tap water for 48 h, decalcifying with Anna Morse solution (10% formic acid:5% sodium citrate, 1:1; Morse, 1945) for 1 week and washing for another 48 h, processing of the bone and surrounding tissue sections was continued by sequential immersion in increasing ethanol concentrations and embedding in paraffin. Serial sagittal sections (5 μm) were made through the lesion, stained with H&E and Mallory and examined by light microscopy for qualitative histological evaluation of inflammation, fibrosis and osteogenesis.

2.14. Histomorphometric analysis

Different adjacent areas, located in the centre of the lesion, were photographed at ×40 magnification. A composite photograph was then prepared, using Corel® Paint Shop Pro v 12, and quantitative measurements were performed using Nikon Image System Elements Basic Research v 3.2 digitalizing software. The centre of the lesion was established at the point where the maximum distance between the cortical lesions was measured, as described by Canettieri *et al*. (2009). For statistical purposes, from that slide, two cuts in front and two behind were selected to be photographed, composed and measured between the bone bridging ends.

The linear distance between the two bone ends was then measured, using the calibrated point-to-point scale present in the Nikon Image System for a magnification obtained with a ×4 objective. These measurements were then recorded in an Excel spreadsheet for later statistical analysis. If the mean differences between the five measurements of each of the two rabbits that were part of the same sample group did not show significant statistical differences in the measurements, then they were used as one group with 10 samples.

2.15. Statistical analysis

Scratch plate and fibroblast proliferation assays were performed in duplicate and the results were expressed as mean SE for $n = 3$. Statistical analysis was performed on the two treatments and the two controls along the increasing doses of CRT, using factorial analysis of variance (ANOVA). For neodermal depth, cell density and re-epithelization morphometric analyses, the values obtained were subjected to the Kruskall–Wallis test for non-parametric samples. A Mann–Whitney test was used for comparison between individual samples. Statistical analyses for all experiments were performed using SPSS v 12 software (Chicago, IL, USA). Statistical analysis was performed to compare the new bone bridging for the different treatments and evaluation times (1, 2 and 4 weeks), by the use of ANOVA and Tukey multiple comparison test (Zar, 1999). Statistical analyses for all experiments were performed using Infostat software (Córdoba, Argentina).

3. Results

3.1. TcCRT is more effective than HuCRT in increasing migration of human fibroblasts in the scratch plate assay

rHuCRT induced a dose-dependent increase in migration of human fibroblasts in the scratch plate assay, with a maximal response of 49.6 ± 8% closure of the wound at 24 h at 20 μg/ml (Figure 3a). Differently from rHuCRT, rTcCRT showed an inverse dose-dependent increment in migration of human fibroblasts, with a peak migration when the lowest concentration (50.9 ± 1.8% at 0.01 μg/ml rTcCRT) was used. However, HuCRT reached a plateau when concentrations > 0.5 μg/ml were used. Both CRT-induced responses were higher than the positive (10% FBS) and negative (MEM) controls ($p = 0.002$), which showed wound area closures of 18.6% and 12.1%, respectively.

3.2. TcCRT is more effective than HuCRT in promoting cellular proliferation of human fibroblasts

40 μg/ml rHuCRT stimulated synchronized subconfluence of human primary dermal fibroblasts in a dose-dependent manner after 48 h of incubation, reaching a 3.9-fold higher effect than the controls at the maximal concentration used (Figure 3b). Differently from HuCRT, rTcCRT showed a maximal effect at 0.01 μg/ml, 3.5-fold higher than the controls, reaching a plateau at 0.1 μg/ml.

DOI: 10.1002/term

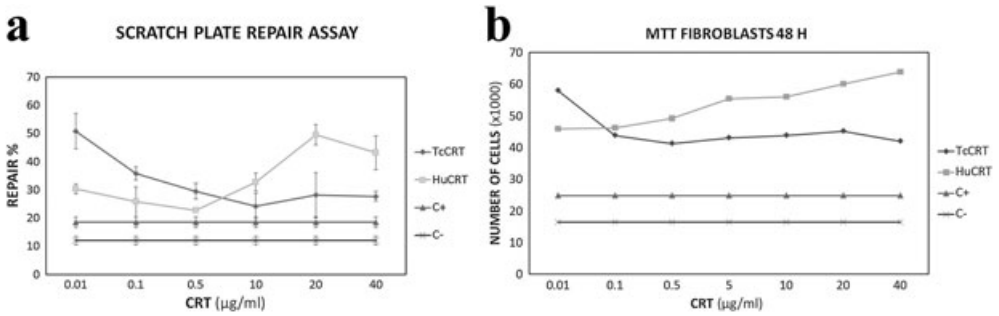

Figure 3. rTcCRT is more effective than rHuCRT in promoting *in vitro* repair and proliferation of fibroblasts. Scratch plate (left) and proliferation assays (right), are shown after 48 h of culture. After incubation, the cells were stained and viewed by inverted light microscopy. Scratch closure (cellular migration) was determined by colouring the cells migrating into the wound areas and calculating the percentage of closure

3.3. Water uptake ability of chitosan sponges

The water uptake ability of the crosslinked chitosan sponges is illustrated in Figure 4. Increasing concentrations of glutaraldehyde, used as crosslinker, correlates with a progressively lower water uptake. 0.5% crosslinker was chosen in order to absorb 40 µl of the CRT solutions for each 20 µg chitosan sponge cube.

3.4. Sponge morphology

A SEM image (Figure 5) shows the highly porous construct of the crosslinked sponge, with multiple open and interconnected 30–200 µm diameter pores and delimited by thin transverse septa.

3.5. Morphological changes on skin wound healing induced by CRT

Dorsal rat skin is formed by subcutaneous panniculus striated muscle, the corium or dermis (connective tissue) and epidermis (epithelium). The epithelial appendages are mostly hair follicles and sebaceous glands. Contrarily to human skin, sweat glands are not observed in rats. The epidermis of the normal rat dorsum is formed by four or five cell thick basal, spinous, granular and cornified layers. Histologically, the dermis is a thick layer of connective tissue composed mainly of collagen fibres, with a low population of cells including adipocytes. At the junction with the epidermis, the dermis forms dermal papillae (Figure 6).

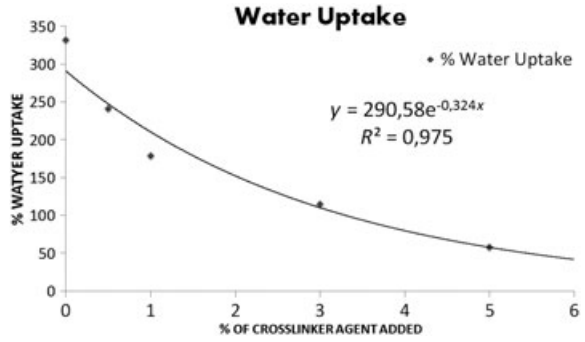

Figure 4. As the degree of glutaraldehyde crosslinking concentration increases, the chitosan matrix water uptake decreases. The swelling ability of glutaraldehyde-crosslinked chitosan sponges was determined by incubating sponges with a crosslinker agent. Increasing concentrations of glutaraldehyde (0–5%) show a progressively lower water uptake. 0.5% crosslinker was chosen in order to absorb 40 µl CRT solution for each 20 µg chitosan sponge cube

When an excisional full-thickness experimental wound is made in the dorsal rat skin, a secondary-intention healing process occurs. After 5 days of normal secondary intention healing, or when a chitosan sponge was implanted subcutaneously under the full-thickness excision, there is still a discontinuity of the subcutaneous panniculus carnosus muscle, with a vascularized granulation tissue filling out the excision space. There is also a demarcation line under the residual fibrin clot, with necrotic debris on the surface of the wound and a thickening of the epidermis at its cut edges, but with no complete re-epithelization process (Figure 7a, c). At 10 days of healing, under normal and chitosan-implanted conditions, partial bridging of the excised pannicular muscle is evident. A more mature dermis is characterized by new intermingled extracellular fibres, with fewer blood vessels and the occurrence of adipocytes. Also, an almost completely finished re-epithelization process, but without hair follicles, sebaceous glands and dermal papillae, can be observed (Figure 7b, d).

On the other hand, CRTs affect the wound-healing processes. In fact, after 5 days of excisional wound healing in the presence of a low dose of TcCRT, a discontinuity of the subcutaneous panniculus muscle was observed. However, an almost mature dermis, with intermingled extracellular fibres and a partially finished re-epithelization process, was observed in spite of the presence of a fibrin clot network on the wound surface (Figure 8a). However, after 10 days, an incipient bridging of the excised pannicular muscle, an almost mature dermis with intermingled extracellular fibres and a completely finished re-epithelization process, including the occurrence of well-developed dermal papillae, was detected (Figure 8b). When comparing low with high doses

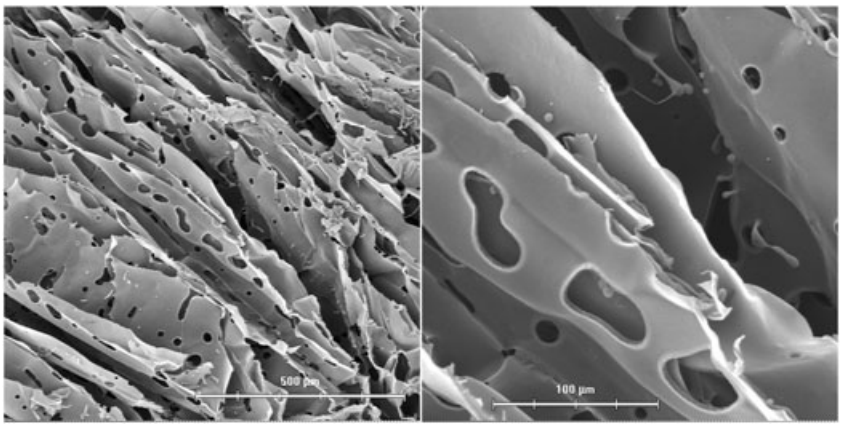

Figure 5. Morphology of a chitosan sponge as seen by scanning electron microscopy. The specimens were coated with a gold layer

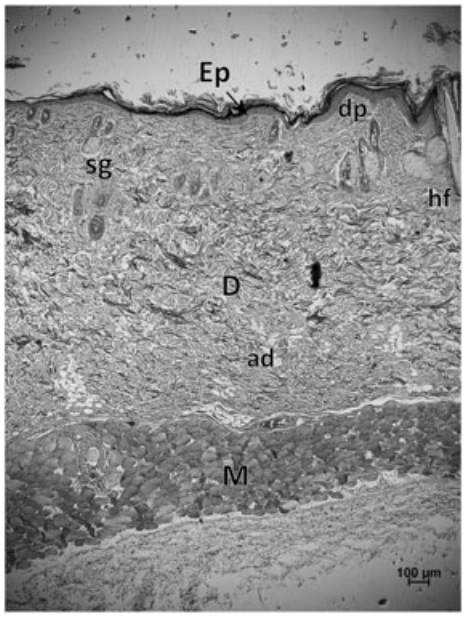

Figure 6. Photomicrograph of a normal dorsal rat skin transverse section. The epidermis (Ep), dermis (D) with hair follicles (hf), sebaceal glands (sg), dermal papillae (dp) and panniculus muscle (M) can be observed; H&E, ×40

of TcCRT after 5 days, the same morphological changes were observed, but with a completely finished re-epithelization process, including the occurrence of abundant hair follicles and sebaceous glands and without fibrin clot network on the surface of the wound (Figure 8c). After 10 days of excisional wound healing in the presence of high-dose TcCRT, a partial bridging of the excised pannicular muscle and a more mature dermis with intermingled extracellular fibres, fewer cells and blood vessels was evident. However, abundant dipocytes and a completely finished re-epithelization process, with an increased number of epithelial cell layers and hyperkeratosis, hair follicles, sebaceous glands and dermal papillae, were present (Figure 8d).

On the other hand, after 5 days of excisional wound healing and a low dose of HuCRT, a discontinuity of the subcutaneous panniculus muscle, a scarce granulation tissue (that did not filled out the excisional space) and a fibrin clot network with necrotic debris on the surface, with no signs of re-epithelization, were apparent (Figure 9a). After 10 days, a discontinuity of the subcutaneous panniculus muscle, an immature vascularized dermis and a residual fibrin clot network on an incipient re-epithelization was observed (Figure 9b), although after 5 days of excisional wounds healing in the presence of high-dose HuCRT, a discontinuity of the subcutaneous panniculus muscle was detected. There was also evidence of mature dermis with interspersed extracellular fibres, fewer cells and blood vessels, together with a completely finished re-epithelization process, including the occurrence of hair follicles and sebaceous glands. Additionally, no fibrin clot network on the surface of the wound was detectable (Figure 9c). After 10 days, full regeneration of the skin, remodelling of muscle healing, maturation of dermis and full re-epithelization of epidermis, increased number of epithelial cells, hyperkeratosis, hair follicles, sebaceous glands and well developed dermal papillae were observed (Figure 9d).

3.6. CRT effect on granulation tissue formation, dermal cell density and re-epithelization

After 5 days of healing in untreated wounds, or those treated with a lower dose of HuCRT, dermal depth reached only 13% of normal (1.5 ± 0.62 mm). CRT-free chitosan sponge-implanted wounds reached 40% of normality, as compared to 75% in those treated with low or high TcCRT doses. However, on treatment of wounds with a higher dose of HuCRT, 100% normality was achieved (Figure 10a). After 10 days of treatment almost all the wounds reached near-normal values of dermal thickness, except with lower doses of both HuCRT and TcCRT, reaching 52% and 66% respectively (Figure 10a).

After 5 days of healing, in almost all wounds the neodermis had a three-fold cell density when compared to normal dermis, except when a CRT-free chitosan or low-dose TcCRT sponges were implanted, reaching almost

DOI: 10.1002/term

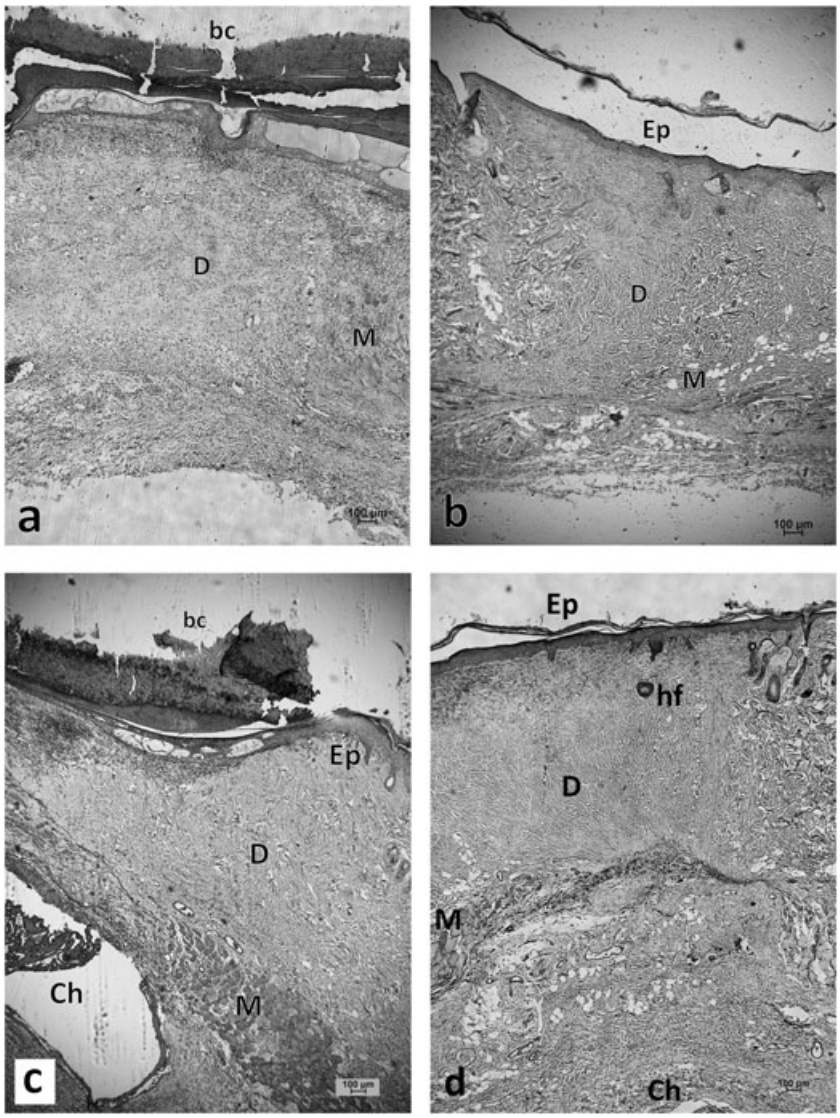

Figure 7. Micrographs of H&E-stained rat skin wounds after 5 (left) and 10 (right) days. Negative control wounds (a, b) and CRT-free chitosan sponges (c, d) can be observed. At 5 days both treatments (a, c), residual blood clots (bc), partial re-epithelization and granulation tissue filling the excisional space (D) can be observed. At 10 days (b, d), both conditions showed a higher degree of maturity in the neodermis (D) and an almost complete re-epithelization (Ep); Ch, chitosan; M, panniculus muscle; hf, hair follicles; ×40

two-fold cell density (Figure 10b). At 10 days, in almost all wounds the neodermis had a significantly higher cell density when compared to normal dermis, except with a low TcCRT dose, which tended to normality, and high-dose HuCRT, which reached normal cell density values (Figure 10b).

After 5 days of healing in untreated and CRT-free chitosan sponge implanted wounds, a significantly low percentage of epithelial resurfacing (percentage re-epithelialized) was observed, while a low HuCRT dose almost completely inhibited re-epithelization. Thus, the low TcCRT dose was more effective than the high dose for epithelial resurfacing. A high HuCRT dose promoted 100% re-epithelization (Figure 10c). After 10 days all the wounds reached normal values of re-epithelization, except with a low HuCRT dose ($37 \pm 4\%$) (Figure 10c).

3.7. CRT inhibits bone defect bridging

When analysing the micrographs of stained decalcified negative control after 1 week, a partial 1.5 mm closure of the original defect can be observed (Figure 11a). After 4 weeks of normal healing of the experimental 5 mm diameter lesion made in the rabbit limbs, new bone tissue bridged the gap (Figure 11b). After 1 week of bone healing in the presence of chitosan implants soaked with high rHuCRT doses, a minimal closure (0.4 mm) of the original defect can be observed (Figure 12a). At 2 weeks, a partial closure ($\pm$ 1.6 mm) of the defect can be observed (Figure 12b). At 4 weeks, the defect shows no appreciable difference from the 2 week micrograph (Figure 12c). After 1 week of bone healing in the presence of chitosan implants soaked with low doses of rTcCRT, a minimal closure

DOI: 10.1002/term

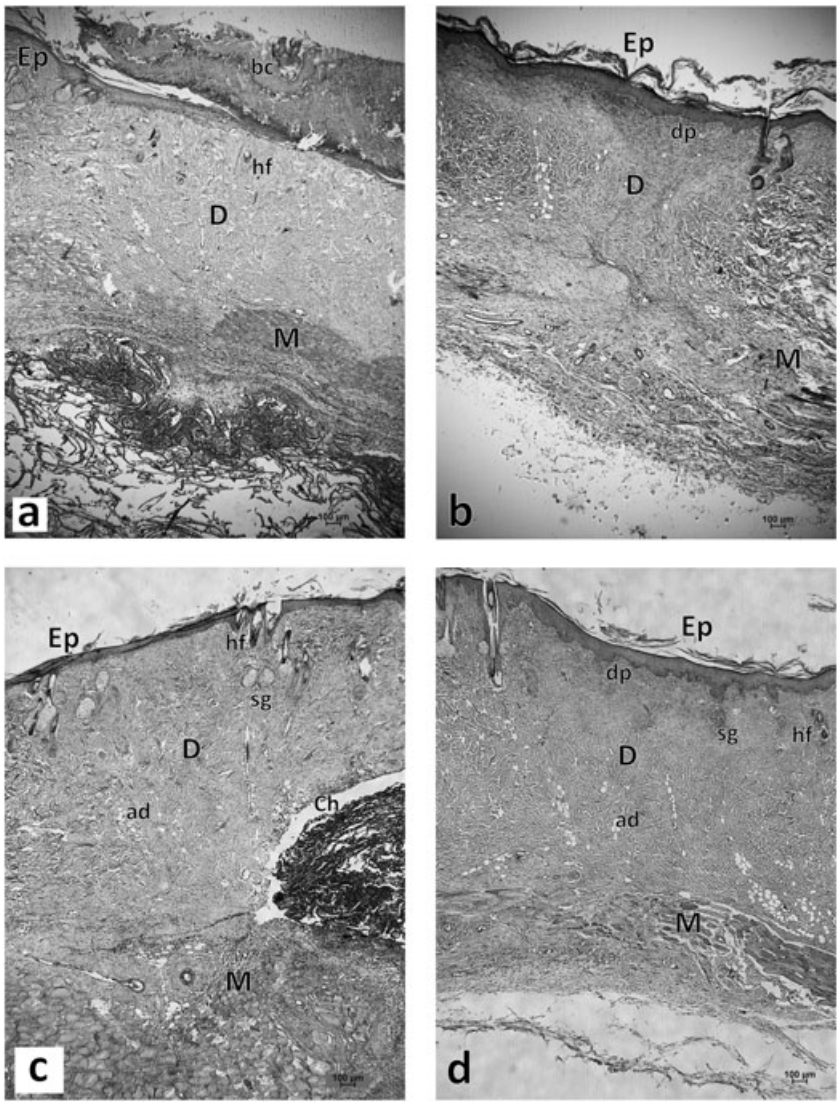

Figure 8. rTcCRT promotes neodermis formation and epithelization. Micrographs of H&E-stained rat skin wounds after 5 (left) and 10 (right) days. Chitosan sponges loaded with low (a, b) and high (c, d) doses of rTcCRT can be observed. At 5 days, the low-dose treatment (a) showed an almost mature neodermis and a partial epithelization process. This is also observed in high-dose treatment (c), but with a complete re-epithelization. At 10 days, the low-dose treatment (b) induced incipient bridging of the pannicular muscle (M), almost mature neodermis (D) with dermal papillae (dp) and re-epithelized epidermis (Ep). The high-dose-treated samples (d) showed partial bridging of the musculature, a more mature neodermis with adipocytes (ad), hair follicles (hf), sebaceous glands (sg) and dermal papillae (dp); ×40

(0.5 mm) of the original defect, similar to the results obtained with high-dose rHuCRT, can be detected. (Figure 13a) At 2 (Figure 13b) and 4 weeks (Figure 13c), a similar ± 1.0 mm closure of the defect is evident. The bone-healing process when only chitosan sponge is implanted showed that, after 1 week, a minimal closure (± 0.3 mm) of the original defect (Figure 14a) was evident. At 2 weeks, a partial closure (± 2 mm) of the defect can be observed (Figure 14b). At 4 weeks, the defect shows a progressive bridging of the bone gap, leaving only a ± 2 mm gap between the bone ends (Figure 14c). As shown in Figure 15, both HuCRT and TcCRT have inhibitory properties on bone bridging. However, CRT from an evolutionarily distant species, such as the protozoan *T. cruzi*, is notoriously (about 400 times) more efficient in this function.

4. Discussion

The role of CRT in healing processes has been well established. Thus, a positive effect of CRT on fibroblasts proliferation and migration has been reported (Gold *et al*., 2006; Nanney *et al*., 2008). These authors show that mammalian (human and rabbit) CRT exerts positive biological effects on both epidermal and dermal healing processes promoting accelerated wound closure and an increased amount of highly cellular granulation tissue. Specifically, *in vitro* and *in vivo* data indicate that CRT acts on cell migration and proliferation into the wound. Dead cells will be removed, extracellular matrix will contribute to wound remodelling and evenly dispersed collagen will reduce scarring. In this regard, the effect on fibroblasts is of utmost interest.

DOI: 10.1002/term

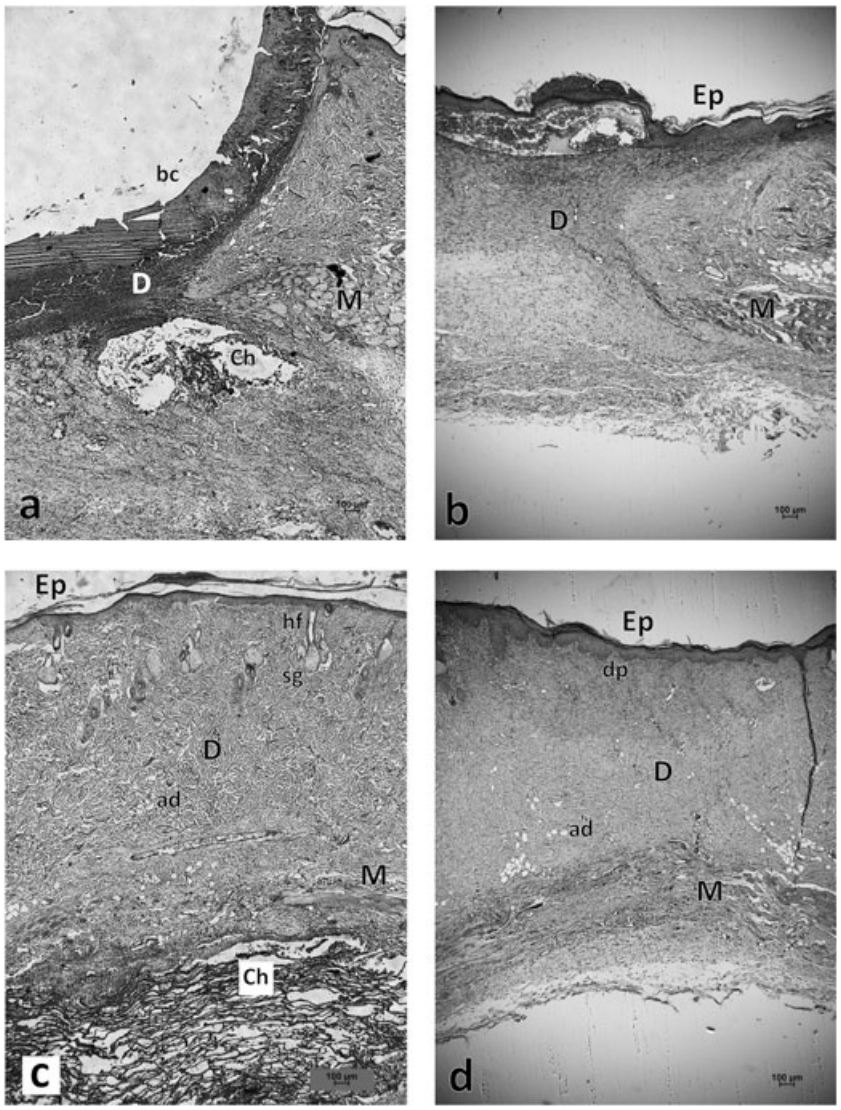

Figure 9. Micrographs of H&E-stained rat skin wounds After 5 (left) and 10 (right) days. Chitosan sponges loaded with low (a, b) and high (c, d) doses of rHuCRT are shown. At 5 days, the low-dose samples (a) showed an almost absent neodermis (D) an abundant blood clot (bc) and no signs of re-epithelization. On the other hand, the high-dose samples (c) showed mature neodermis with adipocytes (ad), hair follicles (hf), sebaceous glands (sg) and dermal papillae (dp), with complete re-epithelization (Ep). This was also observed at 10 days with the high-dose samples (d) but with a complete regeneration of the skin. The low-dose samples (b), in this period, showed an immature vascularized neodermis and a residual blood clot; Ch, chitosan; M, panniculus muscle; ×40

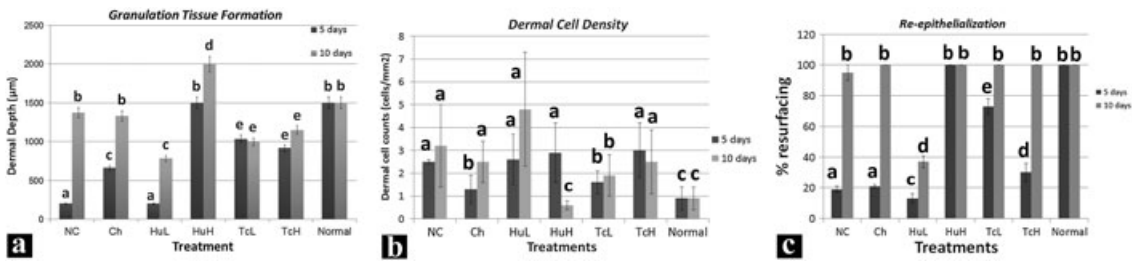

Figure 10. rTcCRT and rHuCRT in low and high concentrations, respectively, promote *in vivo* wound healing at 5 and 10 days after injury. (a) Granulation tissue/neodermal depth measurements (μm), (b) Dermal cell density (cells/mm^2), (c) re-epithelialization (%). Treatments: negative control (NC), where no treatment was applied and CRT-free chitosan sponge (Ch); CRT treatment was in low (L) and high (H) doses (100 ng and 40 μg of rCRT per chitosan sponge, respectively). Four additional experimental groups were generated: HuCRTL, HuCRTH, TcCRTL and TcCRTH. Normal rat skin (Normal) was also included. In each column, values with the same letter are not significantly different, as determined by the least square means test ($p < 0.05$)

DOI: 10.1002/term

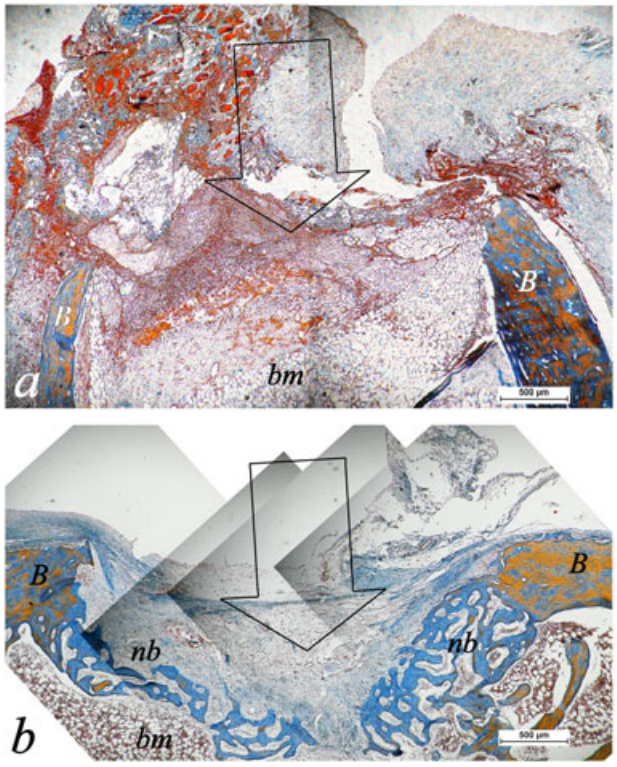

Figure 11. Bone defect closure assessed at 1 and 4 weeks of treatment. Micrographs of Mallory-stained decalcified negative control rabbit bone sections: At 1 (a) and 4 (b) weeks, partial and almost complete closure, respectively, can be observed. Orange (B), mature bone; light blue (nb), new bone; bm, bone marrow tissue; arrows, pathway of the original defect; This figure is available in colour online at wileyonlinelibrary/journal/term; ×40

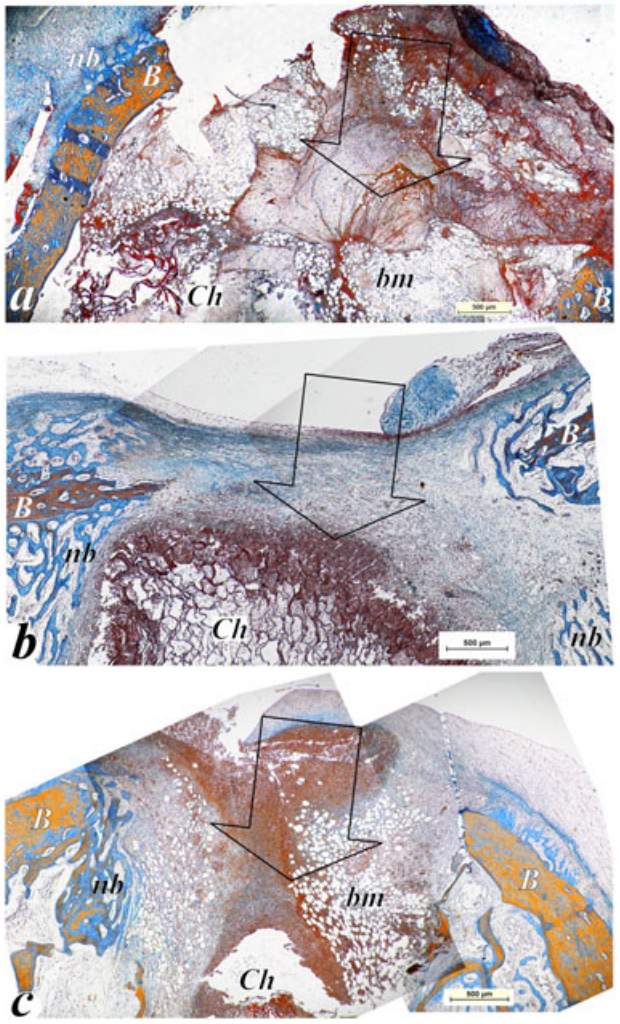

Figure 12. Bone defect closure assessed at 1, 2 and 4 weeks of treatment in the presence of rHuCRT. Micrographs of Mallory-stained decalcified rHuCRT-loaded chitosan sponges in rabbit bone sections: While at 1 week (a) a minimal closure (0.3 mm) of the original defect can be observed, at 2 weeks (b) a partial closure (± 2.0 mm) occurs. At 4 weeks (c) the defect shows no appreciable difference from the 2 week micrograph. Orange (B), mature bone; light blue (nb), new bone; bm, bone marrow tissue; Ch, chitosan sponge; arrows, pathway of the original defect; This figure is available in colour online at wileyonlinelibrary/journal/term; ×40

These cells produce the extracellular matrix granulation tissue, which fills in the skin wound defect and provides the scaffolding for the migration of keratinocytes, essential to re-epithelization. CRT induces an overexpression of TGFβ (Nanney *et al.*, 2008) and an increase in the number of fibroblasts in the healing dermis. Since TGFβ is known for its inductive effects on most matrix proteins needed for attachment and migration of cells (Sporn and Roberts, 1993; O'Kane and Ferguson, 1997; Kinbara *et al.*, 2002), it could be responsible for the acceleration of wound healing. Gold *et al.* (2006) and Nanney *et al.* (2008), in experiments for enhancing wound healing, used repeated treatments directly into the wound in higher concentrations of CRT than those used here.

In spite of the fact that rTcCRT presents a high degree of identity to CRT from humans and other vertebrates (Ferreira *et al.*, 2004a), our *in vitro* study shows interesting differences between these two molecules. In human fibroblast migration, rTcCRT needs 2500 times less concentration than rHuCRT to obtain approximately 50% wound healing *in vitro* (Figure 3a). When analysing fibroblast proliferation *in vitro*, rTcCRT needed 4000 times less concentration to obtain equivalent results (Figure 3b). The results reported here agree with previous ones obtained when the anti-tumour effects of these CRTs were compared (López *et al.*, 2010). These *in vitro* differential effects of CRTs correlate with those obtained *in vivo*. Thus, on equimolar terms, rTcCRT was more effective than rHuCRT in accelerating skin wound healing (Figure 10). An accelerated rate of wound re-epithelialization indicates enhanced wound repair (Nanney *et al.*, 2008). After 5 days of healing, we detected that epithelial islands and epithelial wound edges, in some CRT-treated wounds, display a higher degree of resurfacing and epidermal stratification (Figure 10c). In fact, early wound repair was observed after only 5 days of treatment with high doses of HuCRT and low doses of TcCRT. The presence of mature dermal connective tissue with hair follicles, sebaceal glands and a full-thickness epidermal layer was also evident

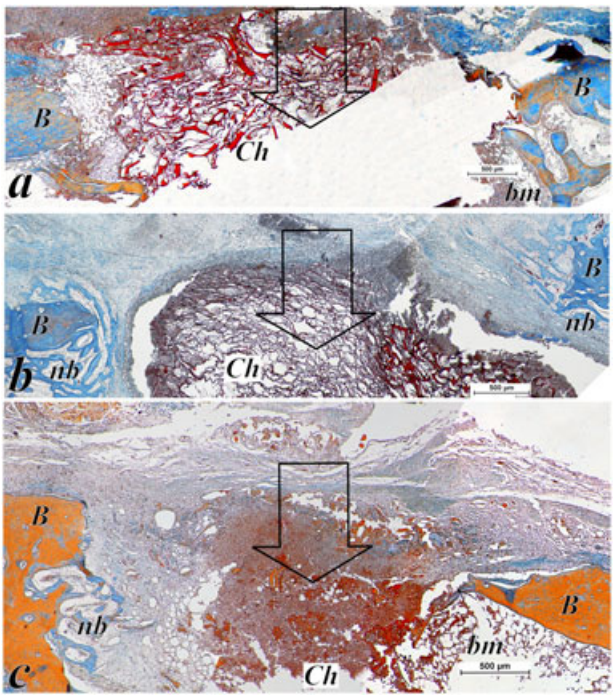

Figure 13. Bone defect closure assessed at 1, 2 and 4 weeks of treatment in the presence of rTcCRT. Micrographs of Mallory-stained decalcified rTcCRT-loaded chitosan sponges in rabbit bone sections: While at 1 week (a) a minimal closure (0.5 mm) of the original defect can be observed, at 2 (b) and 4 (c) weeks a similar 1.5 mm closure of the defect can be observed. Orange (B), mature bone; light blue (nb), new bone; bm, bone marrow tissue; Ch, chitosan sponge; arrows, pathway of the original defect; This figure is available in colour online at wileyonlinelibrary/journal/term; ×40

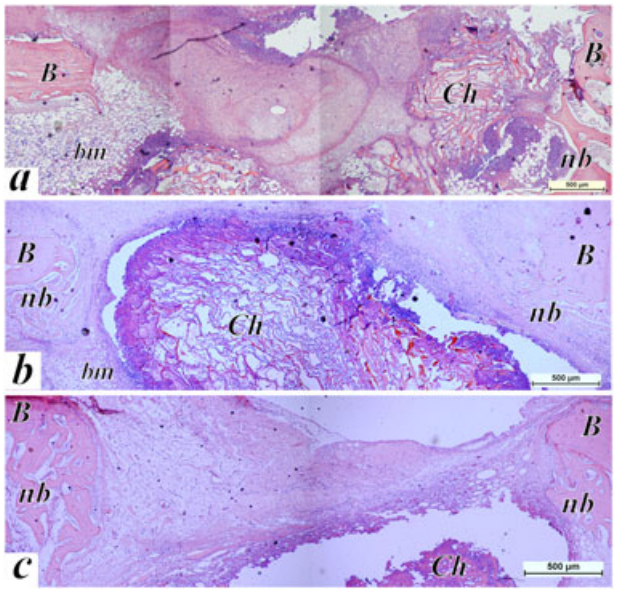

Figure 14. Bone defect closure assessed at 1, 2 and 4 weeks of treatment in the presence of CRT-free chitosan sponges. Representative microphotographs of H&E-stained decalcified chitosan sponges in rabbit bone sections: While at 1 week (a), a minimal closure (0.3 mm) of the original defect can be observed, t 2 (b) and 4 (c) weeks progressive closure of the defect can be observed (2 and 3 mm, respectively); B, mature bone; nb, new bone; bm, bone marrow tissue; Ch, chitosan sponge; arrows, pathway of the original defect; This figure is available in colour online at wileyonlinelibrary/journal/term; ×40

(Figure 9). Whether the differential effect on fibroblast proliferation and spreading and skin wound healing corresponds, among other possibilities, to non-homologous domains of the human and parasite CRTs or, alternatively, to conformational differences, are open questions.

The use of chitosan-based scaffold biomaterials for different tissue engineering applications is well known (Fernandez *et al.*, 2012; Kim *et al.*, 2008). Because of the chitosan swelling behaviour and other biocompatible properties (Yazdani-Pedram *et al.*, 2003), its use as an implant embedded with human or parasite CRTs was explored. Chitosan acts as a slow drug-delivery device, thus increasing the CRT wound-healing efficiency, allowing the use of lower doses and no treatment repetitions. A similar effect could explain the results obtained on bone bridging inhibition, as reported here (Figures 11–13).

It is well known that the critical-sized defect of rabbit limb bones is 8 mm, the smallest size that does not heal spontaneously (Aaboc *et al.*, 1994). Therefore, if any factor added to a < 8 mm unicortical bone defect produces a delay in the bone bridging, this effect should be caused directly by the factor implied. Although we do not know the precise mechanisms by which CRTs affects osteoblast differentiation, here we demonstrate that CRTs inhibit bone bridging *in vivo*. As shown in Figure 15, TcCRT is about 400 times more effective than the human counterpart in delaying bone bridging. The Wnt intracellular signalling pathway controls bone mass (Gong *et al.*, 2001; Glass *et al.*, 2005; Krishnan *et al.*, 2006) and regulates osteoblastogenesis (Bodine and Komm, 2006; Hartmann, 2006), their activity and apoptosis (Bodine *et al.*, 2005). β-Catenin, the intracellular canonical Wnt signalling route (Willert and Nusse, 1998; Kikuchi, 2000; Olkku and Mahonen, 2009), both acts as a transcription factor and, bound to cadherin, regulates cell adhesion and migration. HuCRT alone inhibits Wnt activity *in vitro* in these cells, possibly involving extensive phosphorylation events. Alternatively or concomitantly, HuCRT could, through calcium signalling, modify the nuclear export and calpain-mediated degradation of β-catenin in the cytoplasm (Li and Iyengar, 2002; Benetti *et al.*, 2005). Our results indicate that, in this respect and for still unknown reasons, the parasite-derived molecule (TcCRT) is more efficient, in equimolar terms, than the HuCRT.

In synthesis, recombinant calreticulin from *T. cruzi* is three orders of magnitude more efficient than its human counterpart in its capacity to increase proliferation and migration of human fibroblasts in a wound-healing scratch plate assay, which correlates well with the acceleration of rat skin wound healing and the delay of new bone bridging in rabbits, as reported here. However, new experimental approaches must be tested to use CRT in order to avoid new bone bridging and enhance fibrous tissue for orthopaedic purposes. Also, additional basic research is needed in order

DOI: 10.1002/term

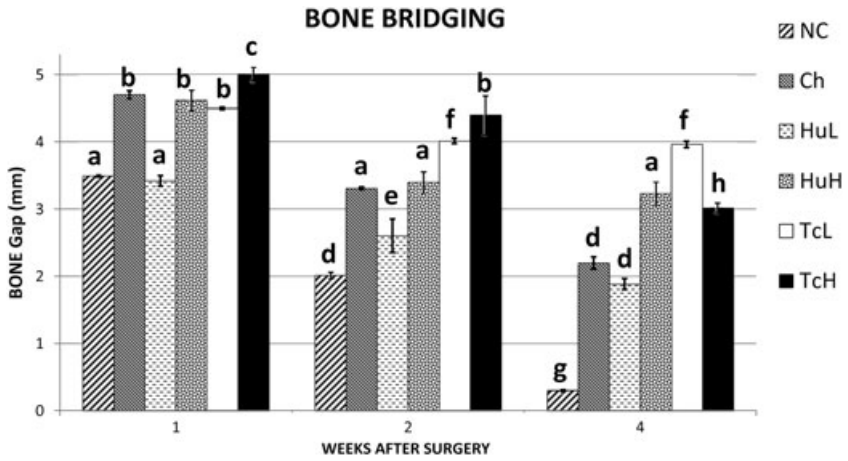

Figure 15. Quantitative analysis of rabbit bone defect bridging is downregulated at high rHuCRT and low rTcCRT concentrations: NC, negative control; Ch, CRT-free chitosan sponge; HuL and HuH, low (100 ng) and high (40 μg) rHuCRT treatments, loaded per chitosan sponge; TcL and TcH, low (100 ng) and high (40 μg) rTcCRT treatments, loaded per chitosan sponge. Experimental times are 1, 2 and 4 weeks after surgery. In each column, values with the same letter are not significantly different, as determined by the least square means test ($p < 0.05$)

to map, in the TcCRT amino acid sequence, the domains responsible for these modulatory activities.

Conflict of Interest

The authors have declared that there is no conflict of interest.

Acknowledgements

This research was supported by the Chilean Council for Science and Technology (CONICYT; Grant Nos FONDECYT 3100021 and 1095095), CONICYT–PBCT (Grant No. ACT 112), VID–Universidad de Chile (Grant No. U-APOYA Línea 1) and Ayuda de Viaje and U-INICIA (Grant No. 11/12-05 2011).

References

Aaboc M, Pinholt EM, Hjörting-Hansen E. 1994; Unicortical critical size defect of rabbit tibia is larger than 8 mm. *J Craniofac Surg* **5**: 201–203.

Aguillón JC, Ferreira L, Pérez C, *et al*. 2000; Tc45, a dimorphic *Trypanosoma cruzi* immunogen with variable chromosomal localization, is calreticulin. *Am J Trop Med Hyg* **63**: 306–312.

Arias JI, González A, Fernández MS, *et al*. 2008; Eggshell membrane as biodegradable bone regeneration inhibitor. *J Tissue Eng Regen Med* **2**: 228–238.

Bae JS, Jang KH, Park SC, *et al*. 2005; Promotion of dermal wound healing by polysaccharides isolated from *Phellinus gilvus* in rats. *J Vet Med Sci* **67**: 111–114.

Bakshandeh N, Siebert JW, Cabrera RC, *et al*. 1992; Isolation and partial characterization of hyaluronan–protein–collagen complex (HA–PC) from fetal sheep skin of different gestational ages. *Biochem Int* **28**: 843–851.

Benetti R, Copetti T, Dell'Orso S, *et al*. 2005; The calpain system is involved in the constitutive regulation of β-catenin signaling functions. *J Biol Chem* **280**: 22070–22080.

Bodine PV, Billiard J, Moran RA, *et al*. 2005; The Wnt antagonist secreted frizzled-related protein-1 controls osteoblast and osteocyte apoptosis. *J Cell Biochem* **96**: 1212–1230.

Bodine PVN, Komm BS. 2006; Wnt signaling and osteoblastogenesis. *Rev Endocr Metab Disord* **7**: 33–39.

Burd DA, Greco RM, Regauer S, *et al*. 1991; Hyaluronan and wound healing: a new perspective. *Br J Plast Surg* **44**: 579–584.

Cabrera RC, Siebert JW, Eidelman Y, *et al*. 1995; The *in vivo* effect of hyaluronan-associated protein–collagen complex on wound repair. *Biochem Mol Biol Int* **37**: 151–158.

Canettieri AC, Colombo CE, Chin CM, *et al*. 2009; Femur bone repair in ovariectomized rats under the local action of alendronate, hydroxyapatite and the association of alendronate and hydroxyapatite. *Int J Exp Pathol* **90**(5): 520–526.

Chagas C. 1909; Nova tripanozomiase humana: estudos sobre a morfolojia e o ciclo evolutivo do *Schizotrypanum cruzi* n. gen., n. sp., ajente etiolojico de nova entidade morbida do homem. *Mem Inst Oswaldo Cruz* **1**: 159–218.

Fernández MS, Arias JI, Martínez MJ, *et al*. 2012; Evaluation of a multilayered chitosan-hydroxy-apatite porous composite enriched with fibronectin or an in vitro-generated bone-like extracellular matrix on proliferation and diferentiation of osteoblasts. *J Tissue Eng Regen Med* **6**(6): 409–504.

Ferreira V, Molina M, Schwaeble W, *et al*. 2005; Does *Trypanosoma cruzi* calreticulin modulate the complement system and angiogenesis? *Trends Parasitol* **21**: 167–174.

Ferreira V, Molina MC, Valck C, *et al*. 2004a; Role of calreticulin from parasites in its interaction with vertebrate hosts. *Mol Immunol* **40**: 1279–1291.

Ferreira V, Valck C, Sanchez G, *et al*. 2004b; The classical activation pathway of the human complement system is specifically inhibited by calreticulin from *Trypanosoma cruzi*. *J Immunol* **172**: 3042–3050.

Glass DA II, Bialek P, Ahn JD, *et al*. 2005; Canonical Wnt signaling in differentiated osteoblasts controls osteoclast differentiation. *Dev Cell* **8**: 751–764.

Gold LI, Eggleton P, Sweetwyne MT, *et al*. 2010; Calreticulin: non-endoplasmic reticulum functions in physiology and disease. *FASEB J* **24**: 665–683.

Gold LI, Rahman M, Blechman KM, *et al*. 2006; Overview of the role for calreticulin in the enhancement of wound healing through multiple biological effects. *J Invest Dermatol Symp Proc* **11**: 57–65.

Gong Y, Slee RB, Fukai N, *et al*. 2001; LDL receptor-related protein 5 (LRP5) affects bone accrual and eye development. *Cell* **16**: 513–523.

Hartmann CA. 2006; Wnt canon orchestrating osteoblastogenesis. *Trends Cell Biol* **16**: 151–158.

Howling GI, Dettmar PW, Goddard PA, *et al*. 2001; The effect of chitin and chitosan on the proliferation of human skin fibroblasts and keratinocytes *in vitro*. *Biomaterials* **22**: 2959–2966.

Kikuchi A. 2000; Regulation of β-catenin signaling in the Wnt pathway. *Biochem Biophys Res Commun* **268**: 243–248.

Kim IY, Seo SJ, Moon HS, *et al*. 2008; Chitosan and its derivatives for tissue engineering applications. *Biotechnol Adv* **26**: 1–21.

Kinbara T, Shirasaki F, Kawara S, *et al*. 2002; Transforming growth factor-β isoforms differently stimulate pro-α2 (I) collagen

gene expression during wound healing process in transgenic mice. *J Cell Physiol* **190**: 375–381.
Krishnan V, Bryant HU, MacDougald OA. 2006; Regulation of bone mass by Wnt signaling. *J Clin Invest* **116**: 1202–1209.
Lai HL, Abu'Khalil A, Craig DQ. 2003; The preparation and characterisation of drug-loaded alginate and chitosan sponges. *Int J Pharm* **251**: 175–181.
Li G, Iyengar R. 2002; Calpain as an effector of the Gq signaling pathway for inhibition of Wnt/β-catenin-regulated cell proliferation. *Proc Natl Acad Sci USA* **99**: 13254–13259.
Lippincott CL. 1992; Femoral head and neck excision in the management of canine hip dysplasia. *Vet Clin N Am Small Anim Pract* **22**: 721–737.
López NC, Valck C, Ramírez G, *et al*. 2010; Antiangiogenic and antitumor effects of *Trypanosoma cruzi* calreticulin. *PLoS Negl Trop Dis* **4**: e730.
Michalak M, Groenendyk J, Szabo E, *et al*. 2009; Calreticulin, a multi-process calcium-buffering chaperone of the endoplasmic reticulum. *Biochem J* **417**: 651–666.
Molina M, Ferreira V, Valck C, *et al*. 2005; An *in vivo* role for *Trypanosoma cruzi* calreticulin in antiangiogenesis. *Mol Biochem Parasitol* **140**: 133–140.
Morse A. 1945; Formic acid–sodium citrate decalcification and butyl alcohol dehydration of teeth and bones for sectioning in paraffin. *J Dent Res* **24**: 143–153.
Nanney LB, Woodrell CD, Greives MR, *et al*. 2008; Calreticulin enhances porcine wound repair by diverse biological effects. *Am J Pathol* **173**: 610–630.
Nguyen DT, Orgill DP, Murphy GF. 2009; *The Pathophysiologic Basis for Wound Healing and Cutaneous Regeneration. Biomaterials for Treating Skin Loss*. CRC Press (USA)/Woodhead Publishing (UK/Europe): Boca Raton, FL/Cambridge, UK; 25–57.
O'Kane S, Ferguson MW. 1997; Transforming growth factor-β3 and wound healing. *Int J Biochem Cell Biol* **29**: 63–78.
Okwueze MI, Cardwell NL, Pollins AC, *et al*. 2007; Modulation of porcine wound repair with a transfected *ErbB3* gene and relevant EGF-like ligands. *J Biochem Cell Biol* **29**: 63–78.
Olkku A, Mahonen A. 2009; Calreticulin mediated glucocorticoid receptor export is involved in β-catenin translocation and Wnt signaling inhibition in human osteoblstic cells. *Bone* **44**: 555–565.
Ostwald TJ, MacLennan DH. 1974; Isolation of a high-affinity calcium-binding protein for sarcoplasmic reticulum. *J Biol Chem* **249**: 974–979.
Palma MM, Fernandez M, Vivanco X, *et al*. 2002; Modulation of androgen receptor protein by culture conditions of human skin fibroblasts. *Int J Androl* **25**: 288–294.
Papp S, Fadel MP, Kim H, *et al*. 2007; Calreticulin affects fibronectin-based cell–substratum adhesion via the regulation of c-Src activity. *J Biol Chem* **282**: 16585–16598.
Ramírez G, Valck C, Ferreira VP, *et al*. 2011a; Extracellular *Trypanosoma cruzi* calreticulin in the host–parasite interplay. *Trends Parasitol* **27**: 115–122.
Ramírez G, Valck C, Molina MC, *et al*. 2011b; *Trypanosoma cruzi* calreticulin: a novel virulence factor that binds complement C1 on the parasite surface and promotes infectivity. *Immunobiology* **216**: 265–273.
Ramos R, Juri M, Ramos A, *et al*. 1991; An Immunogenetically defined and immunodominant Trypanosoma cruzi antigen. *Am J Trop Med Hyg* **44**: 314–322.
Ribeiro CH, López NC, Ramírez GA, *et al*. 2009; Trypanosoma cruzi calreticulin: A possible role in Chagas' disease autoimmunity. *Mol Immunol* **46**: 1092–1099.
Sezer AD, Cevher E, Hatipoğlu F, *et al*. 2008a; Preparation of fucoidan–chitosan hydrogel and its application as burn healing accelerator on rabbits. *Biol Pharm Bull* **31**: 2326–2333.
Sezer AD, Cevher E, Hatipoğlu F, *et al*. 2008b; The use of fucosphere in the treatment of dermal burns in rabbits. *Eur J Pharm Biopharm* **69**: 189–198.
Sezer AD, Hatipoğlu F, Cevher E, *et al*. 2007; Chitosan film containing fucoidan as a wound dressing for dermal burn healing: preparation and *in vitro/in vivo* evaluation. *AAPS Pharm Sci Tech* **8**: 39.
Sporn MB, Roberts AB. 1993; A major advance in the use of growth factors to enhance wound healing. *J Clin Invest* **92**: 2565–2566.
Toledo V, Ramírez G, Valck C, *et al*. 2010; Comparative *in vivo* antiangiogenic effects of calreticulin from *Trypanosoma cruzi* and *Homo sapiens sapiens*. *Biol Res* **43**: 287–289.
Ueno H, Mori T, Fujinaga T. 2001; Topical formulations and wound healing applications of chitosan. *Adv Drug Deliv Ver* **52**: 105–115.
Ueno H, Yamada H, Tanaka I, *et al*. 1999; Accelerating effects of chitosan for healing at early phase of experimental open wound in dogs. *Biomaterials* **20**: 1407–1414.
Valck C, Ramírez G, López N, *et al*. 2010; Molecular mechanisms involved in the inactivation of the first component of human complement by *Trypanosoma cruzi* calreticulin. *Mol Immunol* **47**: 1516–1521.
Willert K, Nusse R. 1998; β-Catenin: a key mediator of Wnt signaling. *Curr Opin Genet Dev* **8**: 95–102.
Yazdani-Pedram M, Tapia C, Retuert J, *et al*. 2003; Synthesis and unusual swelling behavior of combined cationic/non-ionic hydrogels based on chitosan. *Macromol Biosci* **3**: 577–581.
Zar JH. 1999; *Biostatistical Analysis*. Prentice Hall: Upper Saddle River, NJ.